Mathematical Modelling and Analysis
Volume 28, Issue 3, 415–433, 2023
https://doi.org/10.3846/mma.2023.16897

Curvature-Based Characterization of Radial Basis Functions: Application to Interpolation

Mohammad Heidari[a], **Maryam Mohammadi**[a,b] **and Stefano De Marchi**[b]

[a] *Faculty of Mathematical Sciences and Computer, Kharazmi University*
Taleghani Ave. 50, 1561836314 Tehran, Iran
[b] *Department of Mathematics "Tullio Levi-Civita", University of Padova*
Via Trieste, 63-35121 Padova, Italy
E-mail: Std_M.Heidari@khu.ac.ir
E-mail(*corresp.*): m.mohammadi@khu.ac.ir, maryam.mohammadi@unipd.it
E-mail: stefano.demarchi@unipd.it

Received April 29, 2022; accepted June 12, 2023

Abstract. Choosing the scale or shape parameter of radial basis functions (RBFs) is a well-documented but still an open problem in kernel-based methods. It is common to tune it according to the applications, and it plays a crucial role both for the accuracy and stability of the method. In this paper, we first devise a direct relation between the shape parameter of RBFs and their curvature at each point. This leads to characterizing RBFs to scalable and unscalable ones. We prove that all scalable RBFs lie in the $\frac{1}{c^2}$-class which means that their curvature at the point x_j is proportional to $\frac{1}{c_j^2}$, where c_j is the corresponding spatially variable shape parameter at x_j. Some of the most commonly used RBFs are then characterized and classified accordingly to their curvature. Then, the fundamental theory of plane curves helps us recover univariate functions from scattered data, by enforcing the exact and approximate solutions have the same curvature at the point where they meet. This leads to introducing curvature-based scaled RBFs with shape parameters depending on the function values and approximate curvature values of the function to be approximated. Several numerical experiments are devoted to show that the method performs better than the standard fixed-scale basis and some other shape parameter selection methods.

Keywords: radial basis functions, shape parameter, curvature, interpolation.

AMS Subject Classification: 65D05; 65D12; 53Z99.

1 Introduction

Given a set of n distinct points $\{x_j\}_{j=1}^n \subset \mathbb{R}^d$ and corresponding data values $\{f_j\}_{j=1}^n$, the RBF interpolant is given by

$$s(x) = \sum_{j=1}^{n} \lambda_j \phi(\|x - x_j\|), \tag{1.1}$$

where $\phi(r)$, $r \geq 0$, is some radial function, and $\|.\|$ is the Euclidean norm throughout the paper. The expansion coefficients λ_j are determined from the interpolation conditions $s(x_j) = f_j$ for $j = 1, \ldots, n$, which leads to a symmetric linear system $A\lambda = f$, where $A = [\phi(\|x_i - x_j\|)]_{1 \leq i,j \leq n}$. The existence of a solution is assured for positive definite RBFs and also for conditionally positive definite RBFs by adding a lower degree polynomial to (1.1). We can introduce a shape parameter as $\phi\left(\frac{r}{c}\right)$ allowing to scale the basis function ϕ making it flatter as $c \to \infty$ and spiky as $c \to 0$. In order for the system matrix to be well-conditioned, the shape parameter c must not be too large, but large shape parameters are required to obtain better accuracy for the interpolation with RBF (cf. e.g., [16]).

In spatially scaled RBFs the shape parameter varies with the centers getting a more flexible approximation. This means working with functions $\phi\left(\frac{\|x-x_j\|}{c_j}\right)$ for $1 \leq j \leq n$. For more details see [2, 5, 9].

In [1], the scale parameter is considered as a *scale function* and treating it as an additional coordinate. This approach can be fully understood as the standard fixed-scale method applied to a certain sub-manifold of $\mathbb{R}^{d+1}$. For a scale function $c : \mathbb{R}^d \to (0, \infty)$, a *variably scaled kernel (VSK)* can be written as $\phi(\|x - x_j\|^2 + (c(x) - c(x_j))^2)$, in which the tuning of the shape parameter is replaced by the choice of a suitable scale function depending on the data. A question arises: how to find the scale function? Recently, Rossini [14] considered the problem of interpolating functions with gradient faults and tried to provide a strategy to choose a proper scaling function. But it needs the knowledge of the discontinuity curve.

In this paper, we propose an explicit formula for the shape parameter of RBFs based on the value of the curvature in each point. This leads to characterizing RBFs to *scalable* and *unscalable* ones. Some of the most commonly used RBFs are then characterized. Then we use the fundamental theory of plane curves for recovering univariate functions from scattered data by enforcing the exact and approximate solutions have the same curvature at the point where they meet. This leads to introducing curvature-based scaled RBFs.

The paper is organized as follows. In the next section, we provide some basic definitions and theorems from differential geometry [11]. The characterization of RBFs based on the relation between their shape parameter and curvature at each point is outlined in Section 3. In Section 4, curvature-based scaled RBFs are introduced in order to interpolate univariate functions. Some numerical examples are presented in Section 5. The last section is devoted to a brief conclusion and description of future works.

2 Differential geometry basics

Let us consider parametric vector-valued curves $\alpha : [a, b] \subset \mathbb{R} \to \mathbb{R}^n$, $n \geq 1$.

Definition 1. Let $\alpha : [a, b] \to \mathbb{R}^n$ be a regular curve. Then

$$T(t) = \frac{\alpha'(t)}{\|\alpha'(t)\|}, \quad s(t) = \int_a^t \|\alpha'(u)\| \, du,$$

are the unit tangent vector of $\alpha(t)$ and its arc length from a to t, respectively.

Theorem 1. *Let C be a regular plane curve given by $\alpha(t)$. Then the curvature κ of C at t is given by [11]*

$$\kappa[\alpha](t) = \left\| \frac{dT}{ds} \right\|,$$

which measures the rate of change of the unit tangent vector with respect to arc length. It is a measure of how much a curve deviates from a straight line.

The following definition can be simply resulted from the above theorem.

Definition 2. Let $f \in C^2[a, b]$. The curvature of the plane curve $y = f(x)$ with $\alpha(x) = (x, f(x))$ is given by

$$\kappa_f(x) = \frac{|f''(x)|}{(1 + (f'(x))^2)^{\frac{3}{2}}}. \tag{2.1}$$

3 Curvature-based characterization of RBFs

In this section, we present the relation between the spatially variable shape parameter and the curvature of RBFs. Then, we can classify RBFs to scalable and unscalable functions. Hereafter, we assume that $\phi(r)$ is at least in $C^2[0, \infty)$.

Theorem 2. *For spatially variable scaled RBFs*

$$\psi_j(x) = \phi\left(\|x - x_j\|/c_j\right), \quad j = 1, \ldots, n \tag{3.1}$$

we have $\kappa_{\psi_j}(x)\big|_{x=x_j} = \eta/c_j^2$, where η is a positive constant.

Proof. By using Taylor series expansion of ϕ at $r = 0$, we have 2 cases. If ϕ is an infinitely smooth RBF then we have [4, Theorem 10.1]

$$\phi(r) = \sum_{n=0}^{\infty} a_{2n} r^{2n}. \tag{3.2}$$

But, if ϕ is a finitely smooth RBF in $C^{2\delta}[0, \infty), 1 \leq \delta < \infty$, then we get [4, Theorem 10.2]

$$\phi(r) = a_0 + a_2 r^2 + \ldots + a_{2\delta} r^{2\delta} + a_{2\delta+1} r^{2\delta+1} + a_{2\delta+2} r^{2\delta+2} + \ldots, \tag{3.3}$$

or

$$\begin{aligned}\phi(r) = \quad & a_0 + a_2 r^2 + \ldots + a_{2\delta} r^{2\delta} + b_{2\delta} r^{2\delta} \log(r) \\ & + a_{2\delta+2} r^{2\delta+2} + b_{2\delta+2} r^{2\delta+2} \log(r) + \ldots . \end{aligned} \tag{3.4}$$

Now, by considering $\psi(r) = \phi\left(\frac{r}{c}\right)$ in (3.2), (3.3), or (3.4), we have $\psi'(r)|_{r=0} = 0$, $\psi''(r)|_{r=0} = \frac{2a_2}{c^2}$. Then, according to (2.1), we have $\kappa_\psi(r)\,|_{r=0} = \frac{2|a_2|}{c^2}$, which completes the proof by considering $\eta = 2|a_2|$, $r = \|x - x_j\|$. □

Remark 1. As an immediate consequence of Theorem 2, the shape parameter c_j is then given by

$$c_j = \sqrt{\eta/\kappa_j}, \tag{3.5}$$

where, as above, η is a positive constant and $\kappa_j = \kappa_{\psi_j}(x)\,\big|_{x=x_j}$.

In the sequel, we discuss how scalable RBFs are described using Theorem 2.

Definition 3. The radial basis function ϕ is called scalable if it has nonzero curvature at the origin. Otherwise, we call it unscalable.

Remark 2. Scalability means that we can change the curvature of the basis functions (3.1) at the center point x_j by changing the corresponding shape parameter c_j.

Remark 3. It can be noted from Definition 3 that the RBFs which are not at least C^2 at the origin as well as RBFs with zero curvature at the origin are not scalable. They are shape parameter-free.

3.1 Classification of RBFs by curvature

Now, we are going to classify some commonly used RBFs into scalable and unscalable functions. According to Theorem 2, for RBF $\widetilde{\phi}(r)$ we consider $\widetilde{\psi}(r) = \widetilde{\phi}\left(\frac{r}{c}\right)$ and compute its curvature at the origin.

- **Radial Powers**: $\widetilde{\phi}(r) = r^\beta, \beta > 0, \beta \notin 2\mathbb{N}$. Since $\widetilde{\phi}'(r) = \beta r^{\beta-1}$, radial powers are not differentiable at the origin for $0 < \beta \leq 1$. Since $\widetilde{\phi}''(r) = \beta(\beta-1)r^{\beta-2}$, radial powers are not C^2 at the origin for $0 < \beta < 2$ and by using (2.1), we conclude that $\kappa_{\widetilde{\psi}}(r)\Big|_{r=0} = 0$, for $\beta > 2$. Hence, radial powers are unscalable.
- **Thin plate splines (TPS)**: $\widetilde{\phi}(r) = r^{2n}\log(r), n \in \mathbb{N}$. Then,

$$\begin{aligned}\widetilde{\phi}'(r) &= r^{2n-1}\left(2n\log(r) + 1\right), \\ \widetilde{\phi}''(r) &= r^{2n-2}\left(\left(4n^2 - 2n\right)\log(r) + 4n - 1\right)\right).\end{aligned}$$

  Since for $n = 1$, the singularities of the function and first derivative at the origin are removable, but the singularity of the second derivative at the origin is not. TPS are not C^2 at the origin for $n = 1$. Moreover, by

using (2.1), we conclude that $\kappa_{\widetilde{\psi}}(r)\Big|_{r=0} = 0$, for $n \geq 2$. As it happens with radial powers, TPS are unscalable and the use of a shape parameter c with TPS is pointless.

- **Gaussian**: $\widetilde{\phi}(r) = \mathrm{e}^{-r^2}$. We know that the Gaussian is C^∞ at the origin. Since

$$\widetilde{\psi}'(r) = -\frac{2r}{c^2}\mathrm{e}^{-\frac{r^2}{c^2}}, \quad \widetilde{\psi}''(r) = \frac{2}{c^2}\mathrm{e}^{-\frac{r^2}{c^2}}\left(r^2/c^2 - 1\right),$$

using (2.1), we conclude that $\kappa_{\widetilde{\psi}}(r)\Big|_{r=0} = \frac{2}{c^2}$, which leads to $\eta = 2$ in (3.5). Gaussian is then scalable.

- **Generalized Multiquadrics**: $\widetilde{\phi}(r) = \left(1+r^2\right)^\beta$, $\beta \in \mathbb{R}\backslash\mathbb{N}_0$ (if $\beta < 0$ are called inverse multiquadrics) are C^∞ at the origin. Since

$$\widetilde{\psi}'(r) = \frac{2\beta x\left(\frac{r^2}{c^2}+1\right)^{\beta-1}}{c^2}, \quad \widetilde{\psi}''(r) = \frac{2\beta\left((2\beta-1)r^2+c^2\right)\left(\frac{r^2}{c^2}+1\right)^{\beta}}{\left(r^2+c^2\right)^2},$$

using (2.1), $\kappa_{\widetilde{\psi}}(r)\Big|_{r=0} = 2|\beta|\frac{1}{c^2}$, with $\eta = 2|\beta|$ in (3.5). Therefore, they are scalable.

- **Hyperbolic Secant**: $\widetilde{\phi}(r) = \operatorname{sech}(r)$. This function is C^∞ at the origin. Since

$$\widetilde{\psi}'(r) = -\frac{\tanh\left(\frac{r}{c}\right)\operatorname{sech}\left(\frac{r}{c}\right)}{c}, \quad \widetilde{\psi}''(r) = \frac{\tanh^2\left(\frac{r}{c}\right)\operatorname{sech}\left(\frac{r}{c}\right) - \operatorname{sech}^3\left(\frac{r}{c}\right)}{c^2},$$

using (2.1) we obtain $\kappa_{\widetilde{\psi}}(r)\Big|_{r=0} = \frac{1}{c^2}$, which leads to $\eta = 1$ in (3.5).

- **RTH**: It is a new transcendental RBF of the form $\widetilde{\phi}(r) = r\tanh(r)$ introduced for the first time by Heidari et al. [7]. It can be scaled as $r\tanh\left(\frac{r}{c}\right)$ which is a smooth approximant to r with higher accuracy and better convergence properties than the MQ RBF. But, according to Theorem 2, we scale it as $\widetilde{\psi}(r) = \frac{r}{c}\tanh\left(\frac{r}{c}\right)$. This function is C^∞ at the origin. Since

$$\begin{aligned}\widetilde{\psi}'(r) &= \frac{1}{c}\tanh\left(\frac{r}{c}\right) + \frac{r}{c}\operatorname{sech}^2\left(\frac{r}{c}\right),\\ \widetilde{\psi}''(r) &= \left(\frac{2}{c^2} - 2\left(\frac{r}{c^2}\right)\tanh\left(\frac{r}{c}\right)\right)\operatorname{sech}^2\left(\frac{r}{c}\right),\end{aligned}$$

using (2.1) we obtain $\kappa_{\widetilde{\psi}}(r)\Big|_{r=0} = \frac{2}{c^2}$, which leads to $\eta = 2$ in (3.5).

- **Bump function**: $\widetilde{\phi}(r) = \begin{cases} \exp\left(-\frac{1}{1-r^2}\right), & r < 1 \\ 0, & o.w \end{cases}$. This function is

C^∞ at the origin. Since

$$\widetilde{\psi}'(r) = \begin{cases} -2c^2 r \exp\left(-\dfrac{1}{1-(r/c)^2}\right)/(c^2-r^2)^2, & r<c \\ 0, & o.w \end{cases},$$

$$\widetilde{\psi}''(r) = \begin{cases} -2c^2 \exp\left(-\dfrac{1}{1-(r/c)^2}\right)(c^4-3r^4)/\big(c^2-r^2\big)^4, & r<c \\ 0, & o.w \end{cases},$$

using (2.1), we conclude that $\kappa_{\widetilde{\psi}}(r)\Big|_{r=0} = 2\mathrm{e}^{-1}\frac{1}{c^2}$, which leads to $\eta = 2\mathrm{e}^{-1}$ in (3.5).

- **Poisson function**: $\widetilde{\phi}(r) = \dfrac{J_\nu(r)}{r^\nu}$, $\nu = \frac{d}{2}-1$, $d \geq 2$, where J_ν is the Bessel function of the first kind of order ν. While these functions are not defined at the origin, they can be extended to be $C^\infty(\mathbb{R}^d)$ [3]. Since

$$\widetilde{\psi}(r) = \frac{J_\nu(\frac{r}{c})}{(\frac{r}{c})^\nu} = \frac{1}{2^\nu}\sum_{k=0}^{\infty}\frac{(-1)^k r^{2k}}{4^k\ c^{2k}\ k!\ \Gamma(\nu+k+1)},$$

then

$$\widetilde{\psi}'(r) = \frac{1}{2^{\nu-1}}\sum_{k=1}^{\infty}\frac{(-1)^k\ k\ r^{2k-1}}{4^k\ c^{2k}\ k!\ \Gamma(\nu+k+1)},$$

$$\widetilde{\psi}''(r) = \frac{1}{2^{\nu-1}}\sum_{k=1}^{\infty}\frac{(-1)^k\ k\ (2k-1)\ r^{2k-2}}{4^k\ c^{2k}\ k!\ \Gamma(\nu+k+1)}.$$

Again, using (2.1), we conclude that $\kappa_{\widetilde{\psi}}(r)\Big|_{r=0} = \frac{1}{2^{\nu+1}\Gamma(\nu+2)}\frac{1}{c^2}$, which leads to $\eta = \dfrac{1}{2^{\nu+1}\Gamma(\nu+2)}$ in (3.5).

- **Matérn**: $\widetilde{\phi}(r) = r^\nu K_\nu(r)$, $\nu > 0$, where K_ν is the modified Bessel function of the second kind of order ν, that can be defined as a function of the Bessel function of the first kind as follows

$$K_\nu(r) = \frac{\pi}{2}\frac{J_{-\nu}(r)-J_\nu(r)}{\sin(\pi\nu)}, \quad J_\nu(r) = \Big(\frac{r}{2}\Big)^\nu\sum_{k=0}^{\infty}\frac{\big(r^2/4\big)^k}{k!\Gamma(\nu+k+1)}.$$

Then,

$$\widetilde{\psi}(r) = M\Big(\frac{1}{2^{-\nu}}\sum_{k=0}^{\infty}\frac{r^{2k}}{4^k\ k!\ c^{2k}\ \Gamma(-\nu+k+1)} - \frac{1}{2^\nu}\sum_{k=0}^{\infty}\frac{r^{2k+2\nu}}{4^k\ k!\ c^{2k}\ \Gamma(\nu+k+1)}\Big),$$

$$\widetilde{\psi}'(r) = M\Big(\frac{1}{2^{-\nu}}\sum_{k=1}^{\infty}\frac{2k\ r^{2k-1}}{4^k k! c^{2k}\Gamma(-\nu+k+1)} - \frac{1}{2^\nu}\sum_{k=1}^{\infty}\frac{(2k+2\nu)\ r^{2k+2\nu-1}}{4^k\ k!\ c^{2k}\ \Gamma(\nu+k+1)}\Big),$$

$$\widetilde{\psi}''(r) = M\left(\frac{1}{2^{-\nu}}\sum_{k=1}^{\infty}\frac{(2k)(2k-1)\ r^{2k-2}}{4^k\ k!\ c^{2k}\ \Gamma(-\nu+k+1)} - \frac{1}{2^{\nu}}\sum_{k=1}^{\infty}\frac{(2k+2\nu)(2k+2\nu-1)\ r^{2k+2\nu-2}}{4^k\ k!\ c^{2k}\ \Gamma(\nu+k+1)}\right),$$

where $M = \pi/(2\sin(\pi\nu))$. By (2.1) we then have

$$\kappa_{\widetilde{\psi}}(r)|_{r=0} = \frac{1}{c^2}\pi 2^{\nu-2}/|\sin(\pi\nu)\Gamma(-\nu+2)|.$$

Now, the relations

$$\Gamma(\nu+1) = \nu\Gamma(\nu), \quad \Gamma(\nu)\Gamma(1-\nu) = \pi/\sin(\pi\nu) \tag{3.6}$$

lead to $\eta = \frac{2^{\nu-2}\Gamma(\nu)}{|1-\nu|}$ in (3.5).

- **Gaussian-Laguerre**: $\widetilde{\phi}(r) = \mathrm{e}^{-r^2}L_n^{1/2}(r^2)$, where $L_n^{1/2}$ indicates the Laguerre polynomial of degree n and order $1/2$, that is

$$L_n^{1/2}(t) = \sum_{k=0}^{n}\frac{(-1)^k}{k!}\binom{n+1/2}{n-k}t^k.$$

Then,

$$\begin{aligned}
\widetilde{\psi}(r) &= \sum_{k=0}^{n}\frac{(-1)^k}{k!}\binom{n+1/2}{n-k}\frac{r^{2k}}{c^{2k}}\mathrm{e}^{-\frac{r^2}{c^2}},\\
\widetilde{\psi}'(r) &= \sum_{k=1}^{n}\frac{2(-1)^k}{k!}\binom{n+1/2}{n-k}\mathrm{e}^{-\frac{r^2}{c^2}}\left(kc^{-2k}r^{2\,k-1} - c^{-2k-2}r^{2\,k+1}\right),\\
\widetilde{\psi}''(r) &= \sum_{k=1}^{n}\frac{2(-1)^k}{k!}\binom{n+1/2}{n-k}\mathrm{e}^{-\frac{r^2}{c^2}}S,
\end{aligned}$$

where $S = \left(k(2k-1)c^{-2k}r^{2k-2} - c^{-2k-2}(4k+1)r^{2k} + 2c^{-2k-4}r^{2k+2}\right)$.
Using (2.1) $\kappa_{\widetilde{\psi}}(r)\Big|_{r=0} = 2\binom{n+1/2}{n-1}\frac{1}{c^2}$, with $\eta = 2\binom{n+1/2}{n-1}$ in (3.5).

We summarize our findings in Table 1.

4 Interpolating univariate functions via curvature-based scaled radial basis functions

In this section, we intend to recover functions $f : \Omega \subset \mathbb{R} \to \mathbb{R}$, from the set of scattered data $X = \{x_j\}_{j=1}^n$, $F = \{f_j\}_{j=1}^n$, $X \subset \Omega$. At first, the fundamental theorem of curve theory [11] is given, where τ denotes torsion.

Theorem 3. *Two space curves C and C^* with nonzero curvature are congruent (i.e., differ by the composition of a translation and a rotation) if and only if the corresponding arclength parametrizations α, $\alpha^* : [a,b] \to \mathbb{R}^3$ have the property that $\kappa(s) = \kappa^*(s)$ and $\tau(s) = \tau^*(s)$ for all $s \in [a,b]$.*

Table 1. Curvature-based characterization of RBFs: n, β, and ν are RBF parameters.

Name	$\widetilde{\phi}(r)$	$\kappa\left(\widetilde{\phi}\left(\frac{\|x-x_i\|}{c_i}\right)\right)$ at $x=x_i$
Gaussian	$\exp(-r^2)$	$\eta\frac{1}{c_i^2},\ \eta=2.$
Gen. Multiquadrics	$(1+r^2)^{\beta},\quad \beta\in\mathbb{R}\backslash\mathbb{N}_0$	$\eta\frac{1}{c_i^2},\ \eta=2\lvert\beta\rvert$
Hyperbolic Secant	$\operatorname{sech}(r)$	$\eta\frac{1}{c_i^2},\ \eta=1$
RTH	$r\tanh(r)$	$\eta\frac{1}{c_i^2},\ \eta=2.$
Bump function	$\widetilde{\phi}(r)=\begin{cases}\exp\left(-\frac{1}{1-r^2}\right), & r<1,\\ 0, & o.w\end{cases}$	$\eta\frac{1}{c_i^2},\ \eta=2\mathrm{e}^{-1}$
Poisson function	$\frac{J_\nu(r)}{r^\nu},\quad \nu=\frac{d}{2}-1,\ d\geq 2$	$\eta\frac{1}{c_i^2},\ \eta=\frac{1}{2^{\nu+1}\Gamma(\nu+2)}$
Matérn/Sobolev	$r^\nu K_\nu(r),\qquad \nu>0$	$\eta\frac{1}{c_i^2},\ \eta=\frac{2^{\nu-2}\Gamma(\nu)}{\lvert 1-\nu\rvert}$
Gaussian-Laguerre	$\mathrm{e}^{-r^2}L_n^{1/2}(r^2)$	$\eta\frac{1}{c_i^2},\ \eta=2\binom{n+1/2}{n-1}$
Powers	$r^\beta,\qquad 0<\beta\notin 2\mathbb{N}$	unscalable
Thin-plate splines	$r^{2n}\ln(r),\qquad n\in\mathbb{N}$	unscalable

Corollary 1. If $\alpha,\alpha^*: I\longrightarrow\mathbb{R}^2$ are plane curves such that $\kappa_\alpha=\kappa_{\alpha^*}$, then α and α^* are congruent.

Then, the Corollary 1 helps us recover univariate functions from scattered data, by enforcing the exact and approximate solutions have the same curvature at the point where they meet.

Theorem 4. *Let ϕ be a scalable RBF with $\phi(0)\neq 0$, satisfying*

$$\lim_{m\to\infty}\frac{d^k}{dr^k}\phi\left(g(m)r\right)=0,\quad r\neq 0,\quad k=0,1,2, \tag{4.1}$$

where g is a slowly increasing function. Then, for the interpolant

$$s_{\kappa,X,f}(x)=\sum_{j=1}^{n}\alpha_j\psi_j(x)=\sum_{j=1}^{n}\alpha_j\phi\left(\frac{|x-x_j|}{c_j}\right),$$

with

$$c_j=\begin{cases}\sqrt{\eta\,|f_j|/\kappa_j\,|\phi(0)|}, & x=x_j,\\ \\ \frac{1}{g(n)}\sqrt{\eta\,|f_j|/\kappa_j\,|\phi(0)|}, & x\neq x_j,\end{cases} \tag{4.2}$$

η the positive constant appeared in Theorem 2 and $\kappa_j=\kappa_f(x)|_{x=x_j}$, we get

$$\lim_{n\to\infty}\kappa_{s_{\kappa,X,f}}(x)\,|_{x=x_i}=\kappa_i.$$

Proof. Now,

$$s_{\kappa,X,f}(x_i) = \sum_{j=1,j\neq i}^{n} \alpha_j \psi_j(x_i) + \alpha_i \psi_i(x_i) = \sum_{j=1,j\neq i}^{n} \alpha_j \phi\Big(g(n)|x_i - x_j| \times \sqrt{\kappa_j \,|\phi(0)|/\eta\,|f_j|}\Big) + \alpha_i \phi\Big(|x_i - x_i|\sqrt{\kappa_i\,|\phi(0)|/\eta\,|f_i|}\Big).$$

By using (4.1) for $k = 0$ we get

$$\lim_{n\to\infty} |s_{\kappa,X,f}(x_i)| = |\alpha_i \phi(0)|\,.$$

The interpolation condition gives

$$|\alpha_i \phi(0)| = |f_i|\,, \tag{4.3}$$

for sufficiently large n. Now, by considering (2.1), we get

$$\lim_{n\to\infty} \kappa_{s_{\kappa,X,f}}(x)\,|_{x=x_i} = \lim_{n\to\infty} \frac{\left|\frac{d^2}{dx^2}\left(\sum_{j=1,j\neq i}^{n} \alpha_j \psi_j(x) + \alpha_i \psi_i(x)\right)\right|_{x=x_i}}{\left(1+\left(\frac{d}{dx}\left(\sum_{j=1,j\neq i}^{n} \alpha_j \psi_j(x)+\alpha_i \psi_i(x)\right)\right)^2\right)^{\frac{3}{2}}\Bigg|_{x=x_i}}.$$

Then, according to (4.1) and (4.2), the first and second derivatives appeared in the above equation approaches to 0 for $j \neq i$. So,

$$\lim_{n\to\infty} \kappa_{s_{\kappa,X,f}}(x)\,|_{x=x_i} = \frac{\left|\alpha_i\left(\frac{d^2}{dx^2}\phi\left(\sqrt{\frac{\kappa_i|\phi(0)|}{\eta|f_i|}}\,|x-x_i|\right)\right)\right|_{x=x_i}\Bigg|}{\left(1+\left(\alpha_i \frac{d}{dx}\phi\left(\sqrt{\frac{\kappa_i|\phi(0)|}{\eta|f_i|}}\,|x-x_i|\right)\right)^2\right)^{\frac{3}{2}}\Bigg|_{x=x_i}}. \tag{4.4}$$

Now, (4.4) is nothing than with the curvature at the point $x = x_i$ which can be computed by Theorem 2 as

$$\lim_{n\to\infty} \kappa_{s_{\kappa,X,f}}(x)\,|_{x=x_i} = |\alpha_i|\eta/\Big(\frac{\eta|f_i|}{\kappa_i|\phi(0)|}\Big).$$

Therefore, (4.3) results the proof. □

Remark 4. Our theoretical results of Section 3 justify the well-known fact that the classical RBF approximation has difficulty in accurately approximating flat functions [8]. Actually, the curvature of flat functions is almost small and (3.5) leads to large value of the shape parameter c which leads to severe ill-conditioning problem. But, the factor $g(n)$ in (4.2) controls the shape parameter c_j does not become too large. So, in application, we work with the following new scaled RBFs which use a more simple and stable version of (4.2).

Definition 4. Let ϕ be a scalable RBF with $\phi(0) \neq 0$ satisfying (4.1). The curvature-based scaled radial basis functions (CBS RBFs) are defined as

$$\psi_j(x) = \phi\left(|x - x_j|/c_j\right), \tag{4.5}$$

where

$$c_j = \big(1/g(n)\big)\sqrt{\eta\,|f_j|/(\kappa_j\,|\phi(0)|)}. \tag{4.6}$$

So, the RBF interpolant takes the form $s_{\kappa,X,f}(x) = \sum_{j=1}^{n} \alpha_j \psi_j(x)$, where the coefficients α_j are obtained, as usual, by solving the system of linear equations $A\alpha = \mathbf{f}$, where the entries of the interpolation matrix A are given by $A_{ij} = \psi_j(x_i), i, j = 1, \ldots, n$, $\alpha = [\alpha_1, \ldots, \alpha_n]^T$, and $\mathbf{f} = [f_1, \ldots, f_n]^T$. According to Theorem 4, using (4.5) makes the exact and approximate solutions have the same curvature at the point where they meet, for sufficiently large number of data points and avoids from numerical instability according to Remark 4.

In Table 2, we listed those RBFs having conditions of Definition 4.

Table 2. RBFs having conditions of Definition 4.

Name	$\phi(r)$	η
Gaussian	$\exp(-r^2)$	2
Inverse Multiquadrics	$(1+r^2)^{\beta}, \quad \beta \in \mathbb{R},\ \beta < 0$	$2\lvert\beta\rvert$
Hyperbolic Secant	$\operatorname{sech}(r)$	1
Matérn/Sobolev	$r^{\nu}K_{\nu}(r), \quad \nu > 0$	$\dfrac{2^{\nu-2}\Gamma(\nu)}{\lvert 1-\nu\rvert}$
Gaussian-Laguerre	$\mathrm{e}^{-r^2}L_n^{1/2}(r^2)$	$2\binom{n+1/2}{n-1}$

Remark 5. With a spatially variable c_j, the standard proofs for non-singularity of the RBF interpolation matrix A no longer apply. But for small values of c_j ($c_j \to 0$), the A-matrices corresponding to the RBFs in Table 2, will tend to the identity matrix, and non-singularity is obviously assured. Moreover, for large values of c_j ($c_j \to \infty$) the singularities are unlikely to occur [6]. On the other hand, the factor $g(n)$ in (4.6) controls the shape parameter c_j does not become too large.

As an example for the Gaussian, choosing $g(m) = \sqrt{m}$ and knowing that $\phi(0) = 1$, then for $r \neq 0$, we have

$$\begin{aligned}
&\lim_{m\to\infty} \phi\left(\sqrt{m}r\right) = \lim_{m\to\infty} \mathrm{e}^{-\frac{mr^2}{2}} = 0,\\
&\lim_{m\to\infty} \frac{d}{dr}\phi\left(\sqrt{m}r\right) = \lim_{m\to\infty} -mr\mathrm{e}^{-\frac{mr^2}{2}} = 0,\\
&\lim_{m\to\infty} \frac{d^2}{dr^2}\phi\left(\sqrt{m}r\right) = \lim_{m\to\infty} \left(-m\mathrm{e}^{-\frac{mr^2}{2}} + m^2r^2\mathrm{e}^{-\frac{mr^2}{2}}\right) = 0.
\end{aligned}$$

For the Matérn RBF $\phi_\nu(r) = r^\nu K_\nu(r)$, $\nu > 0$, according to the equation

$$\begin{aligned}
r^\nu K_\nu(r) = &\frac{\pi}{2\sin(\pi\nu)}\\
&\times \Big(\frac{1}{2^{-\nu}}\sum_{k=0}^{\infty}\frac{r^{2k}}{4^k k!\Gamma(-\nu+k+1)} - \frac{1}{2^{\nu}}\sum_{k=0}^{\infty}\frac{r^{2k+2\nu}}{4^k k!\Gamma(\nu+k+1)}\Big),
\end{aligned}$$

and the relation (3.6), we have $\phi_\nu(0) = 2^{\nu-1}\Gamma(\nu)$. Furthermore, by the following integral representation

$$\phi_\nu(r) = \frac{\sqrt{\pi}}{2^\nu \Gamma\left(\nu+\frac{1}{2}\right)} r^{2\nu} \int_1^\infty \mathrm{e}^{-rt}\left(t^2-1\right)^{\nu-\frac{1}{2}} dt,$$

for $r \neq 0$, and $g(m) = \sqrt{m}$, we have

$$\lim_{m\to\infty} \phi_\nu\left(\sqrt{m}r\right) = \frac{\sqrt{\pi} r^{2\nu}}{2^\nu \Gamma\left(\nu+\frac{1}{2}\right)} \int_1^\infty \lim_{m\to\infty} m^\nu \mathrm{e}^{-\sqrt{m}rt}\left(t^2-1\right)^{\nu-\frac{1}{2}} dt = 0.$$

Now, since $K'_\nu(r) = -K_{\nu-1}(r) - \frac{\nu}{r}K_\nu(r)$, we have

$$\begin{aligned}
&\lim_{m\to\infty} \frac{d}{dr}\phi_\nu\left(\sqrt{m}r\right) = \lim_{m\to\infty} \frac{d}{dr}\left(\left(\sqrt{m}r\right)^\nu K_\nu\left(\sqrt{m}r\right)\right) = \lim_{m\to\infty} \left((\sqrt{m})^\nu \nu r^{\nu-1}\right. \\
&\left.\times K_\nu\left(\sqrt{m}r\right) + \left(\sqrt{m}r\right)^\nu \sqrt{m} K'_\nu\left(\sqrt{m}r\right)\right) = \lim_{m\to\infty} \left[\left(\sqrt{m}\right)^\nu \nu r^{\nu-1} K_\nu\left(\sqrt{m}r\right)\right. \\
&\left. + \left(\sqrt{m}r\right)^\nu \sqrt{m}\left(-K_{\nu-1}\left(\sqrt{m}r\right) - \frac{\nu}{\sqrt{m}r} K_\nu\left(\sqrt{m}r\right)\right)\right] \\
&= \lim_{m\to\infty} -mr\phi_{\nu-1}\left(\sqrt{m}r\right) \\
&= \frac{\sqrt{\pi} r^{2\nu-1}}{2^{\nu-1}\Gamma\left(\nu-\frac{1}{2}\right)} \int_1^\infty \lim_{m\to\infty} m^\nu \mathrm{e}^{-\sqrt{m}rt}\left(t^2-1\right)^{\nu-\frac{3}{2}} dt = 0.
\end{aligned}$$

Similarly, we can show that $\lim_{m\to\infty} \frac{d^2}{dr^2}\phi_\nu\left(\sqrt{m}r\right) = 0$. The other RBFs in Table 2 can be handled similarly.

Remark 6. The relation (4.6) shows that the shape parameter selection in the univariate RBF interpolation method with scalable RBFs relates to the function values and curvature values of the function to be approximated. Moreover, we can observe the following.

- The scalable RBFs are not good candidates for approximating functions having zero curvature everywhere, like lines. So, one should use the classical fixed-scale RBF interpolation method with an unscalable RBF. Clearly, the power RBF $\phi(r) = r$ is the most appropriate one.
- The classical RBF interpolation method with scalable RBFs may lead to inaccurate solutions for functions having very small values of κ_j.

We discuss these situations in the next section devoted to numerical experiments.

Now, consider the two variable function $f : \mathbb{R}^2 \to \mathbb{R}$. Then, it corresponds with a parametric surface $F : \mathbb{R}^2 \to \mathbb{R}^3$ called the graph of f by $F(x,y) = (x,y,f(x,y))$. The fundamental theorem of surfaces states that the congruent parametric surfaces in $\mathbb{R}^3$ have the same first and second fundamental forms and conversely two parametric surfaces in $\mathbb{R}^3$ with the same first and second fundamental forms are congruent [12]. Discussion about the concepts of the first and second fundamental forms and the methodology of recovering multivariate functions in differential geometry points of view, needs a detailed study, and we leave it to our further work.

5 Numerical results

We now provide some examples that show different roles of the curvature-based scaled RBFs. We take different number of equidistant and Chebyshev-Gauss-Lobatto (CGL) center points in $[a, b]$. We use the maximum absolute error norm $L_\infty = \max_{1\le i\le m} |f_i - \bar{f}_i|$, where f and $\bar{f}$ represent the exact and approximate solutions, respectively. In order to compute interior curvature values $\kappa_j,\ j = 2, \ldots, n-1$, we use the formula for the curvature of the circle which circumscribes the triangle formed by three two-dimensional points (x_{j-1}, f_{j-1}), (x_j, f_j), and (x_{j+1}, f_{j+1}) [13]. That would be an approximation for the curvature at the middle point x_j. The computation goes as follows.

$$
\begin{aligned}
&B = \sqrt{(x_{j-1}-x_j)^2 + (f_{j-1}-f_j)^2}, \quad C = \sqrt{(x_j - x_{j+1})^2 + (f_j - f_{j+1})^2},\\
&D = \sqrt{(x_{j+1}-x_{j-1})^2 + (f_{j+1}-f_{j-1})^2},\\
&S = \frac{1}{2}|(x_j - x_{j-1})(f_{j+1}-f_j) - (f_j - f_{j-1})(x_{j+1}-x_j)|, \quad \kappa_j = \frac{4S}{BCD},
\end{aligned}
$$

where B, C, and D are the lengths of three sides, S is the area of the triangle, and κ_j is the curvature of circumscribing circle. The values of κ_1 and κ_n can be obtained by (2.1) using the following numerical differentiation formulas which are of second-order accuracy [17].

$$
\begin{aligned}
f'(x_1) \approx{}& \left(\tfrac{2x_1-x_2-x_3}{(x_2-x_1)(x_3-x_1)}\right) f_1\\
&+ \left(\tfrac{x_3-x_1}{(x_2-x_1)(x_3-x_2)}\right) f_2\\
&+ \left(\tfrac{x_1-x_2}{(x_3-x_2)(x_3-x_1)}\right) f_3,
\end{aligned}
\qquad
\begin{aligned}
f'(x_n) \approx{}& \left(\tfrac{x_n-x_{n-1}}{(x_n-x_{n-2})(x_{n-1}-x_{n-2})}\right) f_{n-2}\\
&+ \left(\tfrac{x_{n-2}-x_n}{(x_{n-1}-x_{n-2})(x_n-x_{n-1})}\right) f_{n-1}\\
&+ \left(\tfrac{2x_n-x_{n-1}-x_{n-2}}{(x_n-x_{n-1})(x_n-x_{n-2})}\right) f_n,
\end{aligned}
$$

$$
\begin{aligned}
f''(x_1) \approx{}& \left(\tfrac{6x_1-2x_4-2x_3-2x_2}{(x_1-x_2)(x_1-x_3)(x_1-x_4)}\right) f_1\\
&+ \left(\tfrac{-4x_1+2x_4+2x_3}{(x_1-x_2)(x_2-x_3)(x_2-x_4)}\right) f_2\\
&+ \left(\tfrac{4x_1-2x_4-2x_2}{(x_1-x_3)(x_2-x_3)(x_3-x_4)}\right) f_3\\
&+ \left(\tfrac{-4x_1+2x_3+2x_2}{(x_1-x_4)(x_2-x_4)(x_3-x_4)}\right) f_4.
\end{aligned}
\qquad
\begin{aligned}
f''(x_n) \approx{}& \left(\tfrac{-4x_n+2x_{n-1}+2x_{n-2}}{(x_{n-2}-x_{n-3})(x_{n-1}-x_{n-3})(x_n-x_{n-3})}\right) f_{n-3}\\
&+ \left(\tfrac{4x_n-2x_{n-1}-2x_{n-3}}{(x_{n-2}-x_{n-3})(x_{n-1}-x_{n-2})(x_n-x_{n-2})}\right) f_{n-2}\\
&+ \left(\tfrac{-4x_n+2x_{n-3}+2x_{n-2}}{(x_{n-1}-x_{n-2})(x_{n-1}-x_{n-3})(x_n-x_{n-1})}\right) f_{n-1}\\
&+ \left(\tfrac{6x_n-2x_{n-3}-2x_{n-1}-2x_{n-2}}{(x_n-x_{n-2})(x_n-x_{n-1})(x_n-x_{n-3})}\right) f_n.
\end{aligned}
$$

Remark 7. Since division by very small numbers leads to magnification of the absolute error, we use a tolerance σ that one avoids using f_j in (4.6) for each center point with $|f_j| < \sigma$. We also set $\kappa_j = \epsilon_M$ for each center point with $\kappa_j < \epsilon_M$, with $\epsilon_M \approx 2.204e-16$ the machine epsilon.

The optimal shape parameter c for the standard fixed-scale RBF interpolation method is founded by trial end error. In all tests, we took $\sigma = 0.3$ and $m = 125$ equidistant evaluation points. All experiments have been done using an Intel(R) Core(TM) i5-10210U CPU @ 1.60GHz, 2.11 GHz.

5.1 Test problem 1

In the first experiment, we approximate the function (cf. [10])

$$f_1(x) = \sin(4.5x), \quad x \in [0, 1]. \tag{5.1}$$

Absolute errors using the proposed CBS and classical fixed-scale RBFs interpolation methods with the Inverse Quadric RBF ($\beta = -1$), and Gaussian RBF, using $g(n) = \ln(n)$, and 200 equidistant center points are shown in Figures 1, and 2, respectively.

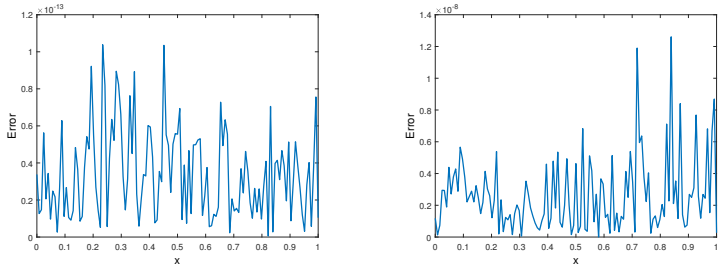

(a) (b)

Figure 1. Absolute errors: (a) CBS RBFs, (b) fixed-scale RBFs, for $n = 200$ equidistant center points with the Inverse Quadric RBF, $g(n) = \ln(n)$, $c = 0.1$; Test problem 5.1.

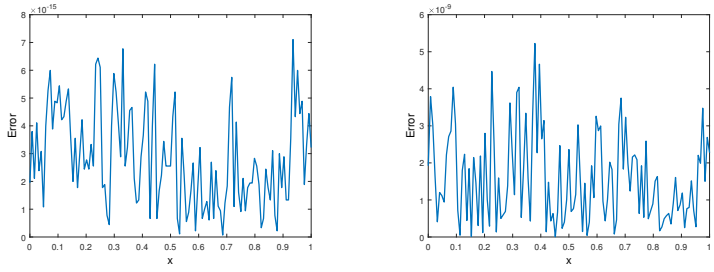

(a) (b)

Figure 2. Absolute errors: (a) CBS RBFs, (b) fixed-scale RBFs, for $n = 200$ equidistant center points with the Gaussian RBF, $g(n) = \ln(n)$, $c = 0.1$; Test problem 5.1.

It should be noted that the results for the CGL center points are the same. Results show that the proposed method leads to more accurate results than the fixed-scale RBFs interpolation method. Furthermore, the numerical errors in Figures 1–2 which are of 10^{-13} and 10^{-15} are really smaller than those reported in [10, p. 904], which is of order 10^{-6} with 1024 center points.

The exact and approximate solutions of $f_1(x)$ and $\kappa(f_1(x))$ using the CBS RBFs interpolation method with the Gaussian RBF are given in Figures 3(a) and 3(b), respectively.

Now, let us change (5.1) into the highly oscillating function

$$f_2(x) = \sin(100x), \quad x \in [0, 2\pi].$$

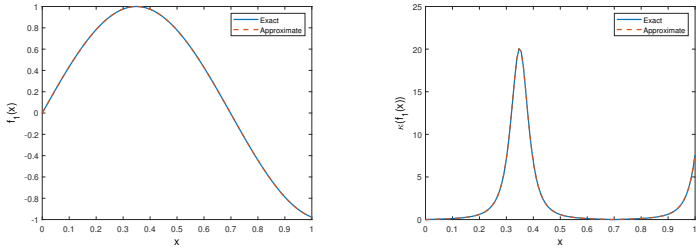

(a) (b)

Figure 3. Exact and approximate solutions of $f_1(x)$ and $\kappa(f_1(x))$ using the CBS RBFs interpolation method for $n = 200$ equidistant center points with the Gaussian RBF, $g(n) = \ln(n)$; Test problem 5.1.

The oscillations make this function have a lot of turning points with zero curvature and a lot of points with very small values of curvature. According to the relation between the curvature values and the shape parameter of RBFs in (4.6), we need to use a little faster growing function $g(n)$. The exact and approximate solutions of $f_2(x)$ and absolute errors using the proposed CBS RBFs interpolation method with the Gaussian RBF, using $g(n) = \sqrt{n}$, and 200 equidistant center points are given in Figures 4(a) and 4(b), respectively.

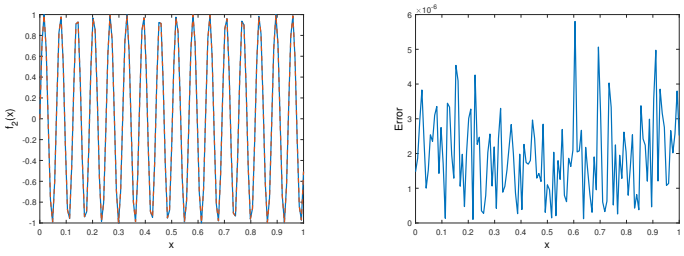

(a) (b)

Figure 4. (a) exact and approximate solutions of $f_2(x)$, (b) absolute errors, using the CBS RBFs interpolation method for $n = 200$ equidistant center points with the Gaussian RBF, $g(n) = \sqrt{n}$; Test problem 5.1.

Plots for 250 CGL center points are also shown in Figures 5(a) and 5(b).

5.2 Test problem 2

The next function we test is (cf. [15])

$$f_3(x) = \arctan(5x) \quad x \in [-1, 1].$$

It is flat near the boundaries but has a steep gradient near $x = 0$. Absolute errors using the proposed CBS and classical fixed-scale RBFs interpolation methods with the Hyperbolic secant RBF, using $g(n) = \sqrt{n}$, $c = 0.09$ and 200, 300 equidistant center points are shown in Figure 6.

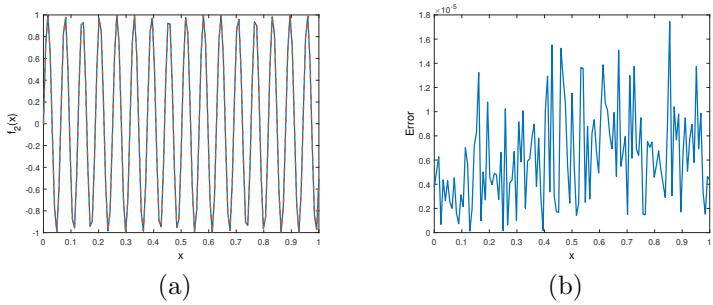

Figure 5. (a) exact and approximate solutions of $f_2(x)$, (b) absolute errors, using the CBS RBFs interpolation method for $n = 250$ CGL center points with the Gaussian RBF, $g(n) = \sqrt{n}$; Test problem 5.1.

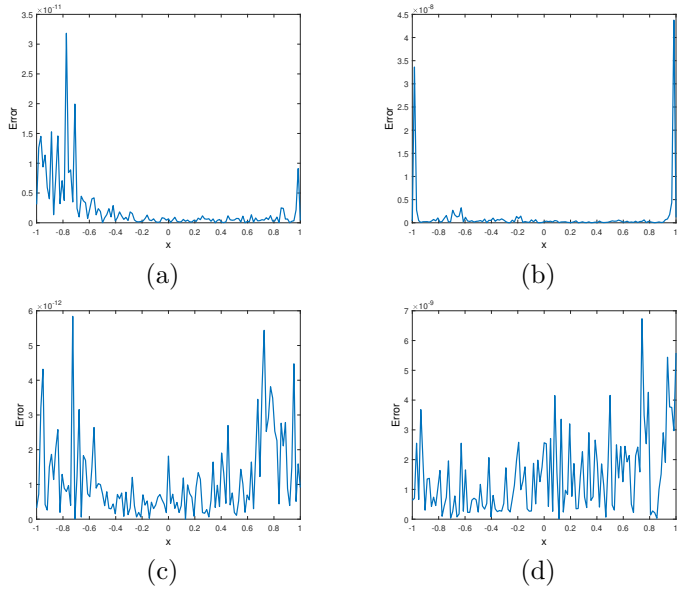

Figure 6. Absolute errors: (a) CBS RBFs, $n = 200$, (b) fixed-scale RBFs, $n = 200$, (c) CBS RBFs, $n = 300$, (d) fixed-scale RBFs, $n = 300$, for equidistant center points with the Hyperbolic secant RBF, $g(n) = \sqrt{n}$, $c = 0.09$; Test problem 5.2.

It is flat near the boundaries but has a steep gradient near $x = 0$. Absolute errors using the proposed CBS and classical fixed-scale RBFs interpolation methods with the Hyperbolic secant RBF, using $g(n) = \sqrt{n}$, $c = 0.09$ and 200, 300 equidistant center points are shown in Figure 6.

Results show that the proposed method leads to more accurate results than the fixed-scale RBFs interpolation method. Moreover, the numerical errors are smaller than those reported in [15] for the random, linearly, and exponentially varying shape parameters.

The exact and approximate solutions of $f_3(x)$ and $\kappa(f_3(x))$ using the CBS RBFs interpolation method with the Gaussian RBF, using $g(n) = \sqrt{n}$, and 200

CGL center points are given in Figures 7(a) and 7(b), respectively.

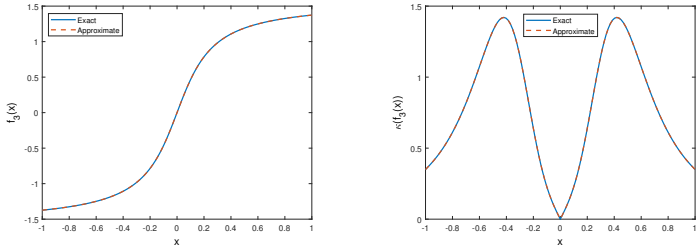

(a) (b)

Figure 7. Exact and approximate solutions of $f_3(x)$ and $\kappa(f_3(x))$ using the CBS RBFs interpolation method for $n = 200$ CGL center points with the Gaussian RBF, $g(n) = \sqrt{n}$; Test problem 2.

5.3 Test problem 3 (Runge function)

In the last example, we consider the Runge function on $[-1, 1]$, that is

$$f_4(x) = \frac{1}{1 + 25x^2}.$$

The L_∞ error norms using the proposed CBS and classical fixed-scale RBFs interpolation methods with the Gaussian RBF, using $g(n) = \sqrt{n}$, $c = 0.08$, and different number of equidistant and CGL center points are reported in Tables 3 and 4, respectively.

Table 3. Comparison of approximation accuracy of CBS and fixed-scale RBFs interpolation methods with the Gaussian RBF for equidistant center points; Test problem 5.3.

	CBS RBF ($g(n) = \sqrt{n}$)			classical RBF ($c = 0.8$)		
n	L_∞	cond	CPUT (s)	L_∞	cond	CPUT (s)
80	6.3×10^{-5}	2.0×10^{19}	0.0351	5.3×10^{-8}	5.4×10^{17}	0.0335
100	8.2×10^{-9}	1.9×10^{18}	0.0370	1.7×10^{-8}	6.1×10^{18}	0.0360
200	1.3×10^{-14}	1.2×10^{19}	0.0457	1.3×10^{-8}	1.0×10^{19}	0.0363
300	1.0×10^{-14}	3.9×10^{19}	0.0541	8.8×10^{-9}	1.8×10^{19}	0.0432

It can be noted from Tables 3–4, that the proposed method leads to more accurate results than the fixed-scale RBFs interpolation method. The exact and approximate solutions of $f_4(x)$ and $\kappa(f_4(x))$ using the CBS RBFs interpolation method for $n = 200$ equidistant center points with the Inverse Multiquadric RBF ($\beta = -\frac{1}{2}$), $g(n) = \sqrt{n}$ are given in Figures 8(a) and 8(b), respectively. In Figure 8(a), we see that no Runge-type oscillations arise. In order to show the important role of the values κ_j in the shape parameter formula (4.6), we multiply 25 by the large number 10^9, and work with

$$f_5(x) = \frac{1}{1 + 25 \times 10^9 \times x^2}.$$

Table 4. Comparison of approximation accuracy of CBS and fixed-scale RBFs interpolation methods with the Gaussian RBF for CGL center points; Test problem 5.3.

	CBS RBF ($g(n) = \sqrt{n}$)			classical RBF ($c = 0.08$)		
n	L_∞	cond	CPUT (s)	L_∞	cond	CPUT (s)
80	3.1×10^{-6}	2.4×10^{18}	0.0455	2.0×10^{-7}	6.2×10^{17}	0.0360
100	7.1×10^{-9}	4.3×10^{18}	0.0438	3.6×10^{-9}	3.4×10^{18}	0.0378
200	1.2×10^{-12}	2.0×10^{19}	0.0467	3.3×10^{-8}	1.8×10^{19}	0.0396
300	8.2×10^{-14}	1.1×10^{19}	0.0519	1.5×10^{-8}	2.3×10^{19}	0.0474

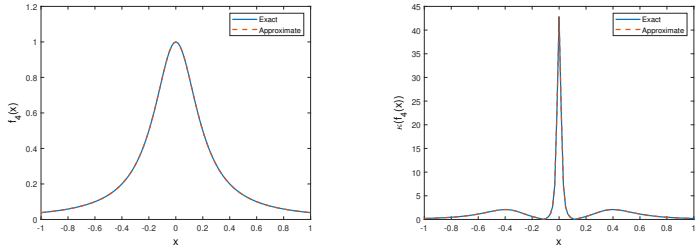

(a) (b)

Figure 8. Exact and approximate solutions of $f_4(x)$ and $\kappa(f_4(x))$ using the CBS RBFs interpolation method for $n = 200$ equidistant center points with the Inverse Multiquadric RBF, $g(n) = \sqrt{n}$; Test problem 5.3.

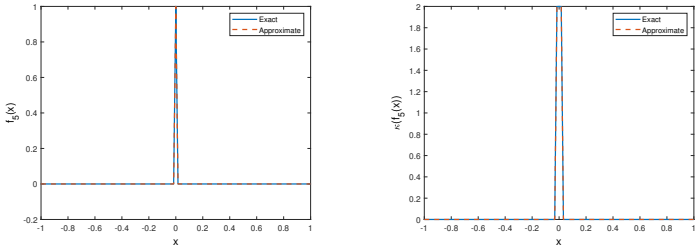

(a) (b)

Figure 9. Exact and approximate solutions of $f_5(x)$ and $\kappa(f_5(x))$ using the CBS RBFs interpolation method for $n = 101$ equidistant center points with the Inverse Multiquadric RBF, $g(n) = \sqrt{n}$; Test problem 5.3.

The exact and approximate solutions of $f_5(x)$ and $\kappa(f_5(x))$ using the CBS RBFs interpolation method for $n = 101$ equidistant center points with the Inverse Multiquadric RBF and $g(n) = \sqrt{n}$ are given in Figures 9(a) and 9(b), respectively. As we can see in Figure 9(b), this change leads to the large value of curvature at the points $x = 0$. Now, we plot the absolute errors using the proposed CBS and classical fixed-scale RBFs interpolation methods with the Gaussian RBF, using the same previous parameters $g(n) = \sqrt{n}$ and $c = 0.08$ in Figure 10. This figure reveals superiority of the proposed method.

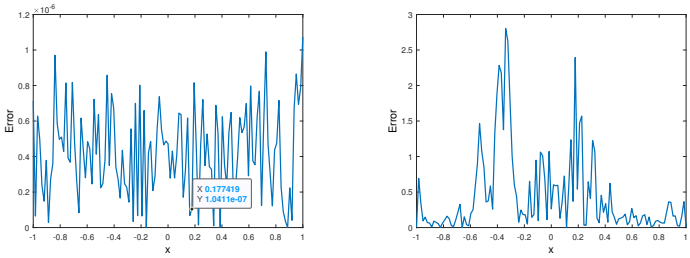

(a) (b)

Figure 10. Absolute errors:(a) CBS RBFs, (b) fixed-scale RBFs, for $n = 101$ equidistant center points with the Gaussian RBF, $g(n) = \sqrt{n}$, $c = 0.08$; Test problem 5.2.

6 Conclusions

In this paper, we first introduce an explicit technique for the shape parameter selection based on the curvature characterization, at $r = 0$, for RBFs. This leads to characterizing RBFs to scalable and unscalable ones. Some of the most commonly used RBFs are characterized and discussed. Then we use the fundamental theory of plane curves for recovering univariate functions from scattered data by enforcing the exact and approximate solutions have the same curvature at the point where they meet. This leads to introducing curvature-based scaled RBFs. Several numerical experiments are devoted to show that the method performs better than the standard fixed-scale basis and some other shape parameter selection methods. In order to generalize the proposed method to higher dimensions, we should work with parametric surfaces and some more tools in differential geometry, like first and second fundamental forms. We leave this to our further works.

Acknowledgements

This research has been accomplished within the Rete ITaliana di Approssimazione (RITA) and the thematic group on Approximation Theory and Applications of the Italian Mathematical Union. We also received the support of GNCS-INδAM. The corresponding author has been also supported by the program "Shaping a World Class University" of the University of Padova, year 2022.

References

[1] M. Bozzini, L. Lenarduzzi, M. Rossini and R. Schaback. Interpolation with variably scaled kernels. *IMA Journal of Numerical Analysis*, **35**(1):199–219, 2015. https://doi.org/10.1093/imanum/drt071.

[2] M. Bozzini, L. Lenarduzzi and R. Schaback. Adaptive interpolation by scaled multiquadrics. *Advances in Computational Mathematics*, **16**(4):375–387, 2002. https://doi.org/10.1023/A:1014584220418.

[3] G.E. Fasshauer. *Meshfree approximation methods with MATLAB*. World Scientific, 2007.

[4] G.E. Fasshauer and M.J. McCourt. *Kernel-based approximation methods using MATLAB*. World Scientific Publishing Company, 2015. https://doi.org/10.1142/9335.

[5] B. Fornberg and J. Zuev. The Runge phenomenon and spatially variable shape parameters in RBF interpolation. *Computers & Mathematics with Applications*, **54**(3):379–398, 2007. https://doi.org/10.1016/j.camwa.2007.01.028.

[6] B. Fornberg and J. Zuev. The Runge phenomenon and spatially variable shape parameters in RBF interpolation. *Computers & Mathematics with Applications*, **54**(3):379–398, 2007. https://doi.org/10.1016/j.camwa.2007.01.028.

[7] M. Heidari, M. Mohammadi and S. De Marchi. A shape preserving quasi-interpolation operator based on a new transcendental RBF. *Dolomites Research Notes on Approximation*, **14**(1):56–73, 2021. https://doi.org/10.14658/pupj-drna-2021-1-6.

[8] E.J. Kansa. Multiquadrics-A scattered data approximation scheme with applications to computational fluid-dynamics-II solutions to parabolic, hyperbolic and elliptic partial differential equations. *Computers & Mathematics with applications*, **19**(8-9):147–161, 1990. https://doi.org/10.1016/0898-1221(90)90271-K.

[9] E.J. Kansa and R.E. Carlson. Improved accuracy of multiquadric interpolation using variable shape parameters. *Computers & Mathematics with Applications*, **24**(12):99–120, 1992. https://doi.org/10.1016/0898-1221(92)90174-G.

[10] L. Ling. A univariate quasi-multiquadric interpolation with better smoothness. *Computers & Mathematics with Applications*, **48**(5):897–912, 2004. https://doi.org/10.1016/j.camwa.2003.05.014.

[11] B. Óneill. Chapter 7 - Riemannian geometry. In *Elementary Differential Geometry (Second Edition)*, pp. 321–387. Academic Press, Boston, 2006. https://doi.org/10.1016/B978-0-12-088735-4.50011-0.

[12] R.S. Palais. *A modern course on curves and surfaces*. Virtual Math Museum, 2011. Available from Internet: `https://virtualmathmuseum.org/Surface/a/bk/curves_surfaces_palais.pdf`.

[13] H. Ratliff. *Cartesian formulas for curvature, circumradius, and circumcenter for any three two-dimensional points*. Zenodo, 2019. https://doi.org/10.5281/zenodo.2556424.

[14] M. Rossini. Interpolating functions with gradient discontinuities via variably scaled kernels. *Dolomites Research Notes on Approximation*, **11**(2):3–14, 2018. https://doi.org/10.14658/pupj-drna-2018-2-2.

[15] S.A. Sarra and D. Sturgill. A random variable shape parameter strategy for radial basis function approximation methods. *Engineering Analysis with Boundary Elements*, **33**(11):1239–1245, 2009. https://doi.org/10.1016/j.enganabound.2009.07.003.

[16] R. Schaback. Error estimates and condition numbers for radial basis function interpolation. *Advances in Computational Mathematics*, **3**(3):251–264, 1995. https://doi.org/10.1007/BF02432002.

[17] A.K. Singh and B.S. Bhadauria. Finite difference formulae for unequal subintervals using Lagrange's interpolation formula. *International Journal of Mathematical Analysis*, **3**(17):815–827, 2009.